A functional interaction between TDP-43 and USP10 reveals USP10 dysfunction in TDP-43 proteinopathies

Marrero-Gagliardi A[1,2 #], Noda J[1, #], Zanovello M[2], Gerenu G[3,4], Brito Armas JM[1], Bampton A[2], Torres P[5], Hernández-Eguiazu H[3], Moragón S[3], Pellegrini F[2], Pérez Hernández C[1], Fumagallo F[1], Taoro-González L[1], Muñoz de Bustillo Alfaro R[1], Brown AL[2],Quinet G[6], Andrés-Benito P[7], Ferrer I[8], Acebes A[9], Freire R[10], Smits VAJ[10], Gil-Bea FJ[3,4], Keuss MJ[2], Portero-Otin M[5], Lashley T[2], Fratta P[2], Acevedo-Arozena A[1*]

1. Canary Islands University Hospital Research Unit, IISC, ITB-ULL and CIBERNED, La Laguna, Tenerife, Spain
2. UCL Institute of Neurology, University College London, UK
3. Department of Neuroscience, BioGipuzkoa Health Research Institute (IIS BioGipuzkoa), CIBERNED, San Sebastian, Spain.
4. IKERBASQUE Basque Foundation for Science, Bilbao, Spain
5. Biomedical Research Institute (IRBLleida), University of Lleida (UdL), Lleida, Spain
6. Canary Islands University Hospital Research Unit/FIISC, ITB-ULL, Spain
7. Bellvitge Institute for Biomedical Research (IDIBELL), CIBERNED, L'Hospitalet de Llobregat, Spain
8. Bellvitge Institute for Biomedical Research (IDIBELL), CIBERNED, L'Hospitalet de Llobregat, and Department of Pathology and Experimental Therapeutics, University of Barcelona, Spain
9. University of La Laguna, ITB-ULL, Spain
10. Canary Islands University Hospital Research Unit/FIISC, ITB-ULL, Universidad Fernando Pessoa Canarias, Spain

# These authors contributed equally to this work

* Corresponding author: aacevedo@ull.edu.es

ABSTRACT

Amyotrophic lateral sclerosis (ALS) and frontotemporal dementia (FTD) are fatal neurodegenerative disorders characterised by the progressive degeneration of specific neurons, that are defined by the appearance of TDP-43 pathology leading to TDP-43 cytoplasmic aggregation coupled with its nuclear loss. Although the causes of TDP-43 pathology in TDP-43 proteinopathies remain unclear, stress response may play a significant role, with some TDP-43 co-localizing with stress granules (SG). The ubiquitin-specific protease 10 (USP10) is a critical inhibitor of SG assembly. Here, we identify a new functional interaction between TDP-43 and USP10, with both proteins modulating different key aspects of the biology of the other. Adding to their functional connection, we assign a new function to USP10 as a modulator of alternative splicing, sharing a subset of splicing targets with TDP-43. Critically, we found that USP10 levels can increase in postmortem tissue from ALS and FTD patients and that USP10 can ameliorate TDP-43 mediated toxicity *in vivo* in an animal model, overall suggesting a new role for USP10 in TDP-43 proteinopathies.

INTRODUCTION

Amyotrophic lateral sclerosis (ALS) is a fatal neurodegenerative disease characterised by the progressive degeneration of motor neurons in the cerebral cortex, brainstem and spinal cord, with a rapid progression from diagnosis to death of typically less than five years (1). ALS shares genetic and pathological features with the neurodegenerative disorder frontotemporal dementia (FTD). Approximately 20% of people with ALS meet the clinical criteria for a diagnosis associated with FTD (2). Both diseases share genetic, clinical and pathological features, with each representing the extremes of a broad disease spectrum (1,3). TDP-43 is a ubiquitously expressed and predominantly nuclear RNA/DNA binding protein encoded by the *TARDBP* gene that is involved in multiple aspects of RNA processing through its RNA binding capacity (4,5). TDP-43 plays a central role in ALS and FTD pathogenesis as a major component of the proteinaceous inclusions that pathologically define the great majority (>95%) of ALS cases and that are present in up to 50% of FTD cases (1,6). TDP-43 pathology occurs when TDP-43 is depleted from the nucleus and is sequestered as hyperphosphorylated insoluble aggregates in the cytoplasm, nucleus and/or dystrophic neurites of affected neurons. These features are also present in all cases of the dementia entity limbic-predominant age-related TDP-43 encephalopathy (LATE) and up to 50% of Alzheimer's disease (AD) cases, which along with other disorders exhibiting similar TDP-43 pathology are collectively known as TDP-43 proteinopathies (7). The cytoplasmic aggregation of TDP-43 confers a loss of nuclear function, causing pleiotropic defects including splicing dysregulation such as the expression of toxic cryptic exons (8). Additionally, a possible toxic gain-of-function due to cytoplasmic mislocalization can

contribute to the further nuclear clearance of TDP-43 and other RNA binding proteins (RBPs) (9–12).

TDP-43 and other RBPs involved in ALS, such as FUS, are components of stress granules (SG) - membraneless macromolecular ribonucleoprotein cytoplasmic condensates that are formed in response to different cellular stresses. Although the function of SG is not fully understood, they likely promote cell survival under stress conditions by storing stalled translation components, including mRNAs, RBPs, ribosomal components and initiation factors (13–15). For their formation, SG are thought to require an increase in cytoplasmic free RNA concentrations to promote the condensation of the core SG protein G3BP1 (16,17). Interestingly, TDP-43 controls *G3BP1* levels through direct mRNA binding, modulating SG formation (18–21). A key protein in the regulation of SG assembly is the ubiquitin-specific peptidase 10 (USP10), which inhibits SG formation by negatively influencing G3BP1 cooperativity via direct binding, in an interaction with G3BP1 that is mutually exclusive with that of Caprin1, which promotes SG formation (16, 17, 22–24). USP10 is a multifunctional protein with several roles that could be dependent on its enzymatic deubiquitinase activity, including controlling the levels of critical proteins like p53 or AMPK (25) and ribosome quality control (26,27), or independent of this activity, such as the inhibition of SG formation (16,17).

Recently, USP10 has been associated with different neurodegenerative conditions, colocalizing with tau aggregates in AD patients and is thought to promote tau aggregation in neuronal cells exposed to stress (28). In a cellular model of TDP-43 proteinopathy, USP10 promotes the elimination of TDP43-positive SG upon proteasome inhibition, whilst USP10 downregulation promotes the accumulation of TDP-43 insoluble fragments in the cytoplasm (29). Furthermore, USP10 was identified as a modifier of C9Orf72 toxicity in *Drosophila* (30).

Here, using different cellular models of TDP-43 cytoplasmic mislocalization to search for aggregation suppressors, we found that USP10 inhibits the formation of TDP-43 cytoplasmic inclusions through a mechanism that requires USP10 interaction with G3BP1. In different cellular models, we went on to study the effects of USP10 in modulating other aspects of TDP-43 biology, including its expression and splicing functionality. Furthermore, we discovered that USP10 can, on its own, modulate transcriptome-wide alternative splicing, with a clear overlap with some TDP-43 splicing targets. Critically, we show that USP10 can rescue TDP-43 associated toxicity *in vivo* in a *Drosophila* model. Finally, we found that, in turn, TDP-43 can also control different aspects of USP10 biology, including its expression, which we determined is dysregulated in ALS and FTD patients, further implicating USP10 in the pathogenesis of TDP-43 proteinopathies.

RESULTS

USP10 controls TDP-43 aggregation

To test the effects of USP10 on TDP-43 cytoplasmic aggregation, the cardinal feature of TDP-43 proteinopathies, we first used a cellular model in HeLa cells transfected with a construct carrying a GFP-tagged TDP-43 harbouring mutations in its nuclear localization signal (NLS) (GFP_TDP-43$^{\Delta NLS}$), leading to its mislocalization and the formation of cytoplasmic aggregates (31). Co-transfecting GFP_TDP-43$^{\Delta NLS}$ with USP10 resulted in a major decrease in both the size and the percentage of cells with TDP-43 cytoplasmic inclusions when compared to the effects of GFP_TDP-43$^{\Delta NLS}$ alone (GFP-ΔNLS, Fig. 1A). USP10 overexpression levels were controlled via western blots (Fig. S1A). To ensure that these results were not dependent on cell type, we performed the same experiments in U2OS and SH-SY5Y cell lines, largely confirming the results from Hela (Fig. S1B, C). We also tested the effects of USP10 downregulation, co-transfecting the GFP_TDP-43$^{\Delta NLS}$ construct

with siRNAs against *USP10*. Reassuringly, USP10 downregulation led to the opposite results obtained when USP10 was upregulated, causing an increase in the size of TDP-43 inclusions when co-transfected with GFP_TDP-43$^{\Delta NLS}$ (Fig. S1D).

Given that TDP-43 and other RBPs associated with ALS can accumulate in SG (32,33) and knowing that USP10 inhibits SG assembly (16,17), we wondered whether the effects of USP10 on TDP-43 aggregation might be mediated by USP10's role in regulating SG formation. Thus, in the same Hela cellular model transfected with GFP_TDP-43$^{\Delta NLS}$, we also quantified SG by immunocytochemistry using antibodies against G3BP1. As expected for a known inhibitor of SG formation, USP10 co-transfection with GFP_TDP-43$^{\Delta NLS}$ led to a clear reduction in SG size and a decrease in the number of cells with SG when compared with the co-transfection with the empty vector (EV) (Fig. 1A). In this model, the colocalization between TDP-43 cytoplasmic foci and SG was very high, as the expression of the cytoplasmic GFP_TDP-43$^{\Delta NLS}$ construct itself leads to SG formation (Fig. S1E).

Because of the almost complete colocalization between TDP-43 and G3BP1 in this experimental setting, it was not possible to distinguish between USP10's roles as a generic SG formation inhibitor from its possible effects on TDP-43 aggregation. To directly address if USP10 could affect TDP-43 aggregation independently of its co-localization in SG, we turned to a different cellular model in which the endogenous *TARDBP* gene is edited to harbour a disrupted NLS and a fluorescent tag (TDP-43$^{\Delta NLS}$-Clover) expressed under a doxycycline-inducible system that lead to TDP-43 cytoplasmic aggregation under oxidative stress conditions (12). Under these conditions, SG and TDP-43 foci were both formed and were largely independent, allowing to assess the effects of USP10 specifically on endogenous TDP-43 aggregates that do not colocalize with SG (Fig. 1B and S1E). In this model, USP10 overexpression, when compared to the EV control, also led to a decrease in the percentage of cells with TDP-43 inclusions as well as in the number of TDP-43 inclusions per cell (Fig.

1B). USP10 overexpression levels were controlled via western blots (Fig. S1A). Similar results were also obtained in a third cellular model, on which SH-SY5Y cells were treated with oxidative and osmotic stress, again assessing endogenous TDP-43 inclusions (Fig S1F).

Thus, USP10 can modulate TDP-43 aggregation in all tested conditions, irrespective of the cause of aggregation and independently of its colocalization with stress granules.

The effect of USP10 on TDP-43 cytoplasmic aggregation is independent of its deubiquitinase activity, but dependent on its binding to G3BP1

USP10's deubiquitinase activity is critical for its involvement in regulating different cellular processes (24, 34–36), but not for the regulation of SG formation (16). Thus, to begin to determine the mechanisms by which USP10 inhibits TDP-43 aggregation, we used the same two distinct cellular models (the overexpression of GFP_TDP-43$^{\Delta NLS}$ in HeLa cells, as well as the inducible TDP-43$^{\Delta NLS}$-Clover U2OS model), to test the effects of a mutated version of USP10 devoid of its catalytic activity (USP10^{C424A}) (37, 38). The expression of enzymatically inactive USP10^{C424A} led to a decrease in TDP-43 aggregation that was indistinguishable from that of USP10^{WT} in both cellular models (Fig. 1C, D), showing that USP10 effects on TDP-43 aggregation are not dependent of its deubiquitinase activity.

We then tested for a possible role of the interaction between USP10 and G3BP1 on USP10´s capacity to clear TDP-43 aggregates by using a USP10^{F10A} mutant that loses its ability to bind G3BP1 (24). As already published in other contexts (16), USP10^{F10A} overexpression, did not inhibited SG formation in our co-transfection model with GFP_TDP-43$^{\Delta NLS}$ (Fig. S1G). We also confirmed by immunoblot that all USP10 constructs were expressed at similar levels (Fig. S1H). Crucially, unlike USP10^{WT} or USP10^{C424A}, USP10^{F10A} had no significant effects on TDP-43 aggregation in any of the models, suggesting that the inhibitory role of USP10 on TDP-43 aggregation is mediated by its interaction with G3BP1 (Fig. 1C, D). Overall, these

results show that USP10 binding to G3BP1 is required for its inhibition of TDP-43 aggregation in a manner that is not dependent on TDP-43 colocalization with SG.

USP10 enhances TDP-43 functionality on splicing

Next, we tested whether USP10 could affect TDP-43 functionality at the mRNA splicing level. First, we employed a widely used *CFTR* reporter minigene in which TDP-43 function is known to modulate the inclusion/exclusion ratio of *CFTR* exon 9 (39). We co-transfected the *CFTR* minigene together with USP10 in HeLa cells and assessed the percentage of exclusion (PSE) of *CFTR* exon 9. Our results show that USP10 overexpression enhance endogenous TDP-43 splicing function when compared to the EV (Fig. 2A).

In addition to the *CFTR* reporter minigene, we also assessed the PSE of endogenous exons known to be controlled by TDP-43 function, such as *RABGEF* exon 16 and *RWDD1* exon 2. In agreement with the minigene data, USP10 overexpression caused an increase in TDP-43 splicing function on both targets when compared to the EV controls (Fig. 2B and Fig. S2A). We obtained similar results in U2OS (Fig. S2B), demonstrating that, independently of the cell line, USP10 can positively modulate TDP-43 splicing function. This enhancement of TDP-43 splicing function upon USP10 overexpression occurs without affecting endogenous TDP-43 expression levels (Fig. S2C). However, acute USP10 downregulation in U2OS cells caused a small but significant reduction in endogenous TDP-43 protein when compared to the siRNA control (Fig. 2C), without affecting *TARDBP* mRNA levels. Thus, USP10 can modulate TDP-43 splicing functionality and protein expression levels.

USP10 affects alternative splicing overlapping with events controlled by TDP-43

As we show that USP10 can enhance TDP-43 splicing function, we wondered whether USP10 could, on its own, affect transcriptome-wide alternative splicing. Thus, we performed RNA-sequencing (RNAseq) analysis on HeLa cells transfected with USP10 and compared to

an EV control. Indeed, USP10 significantly affected the inclusion of around 500 alterative splicing events (Fig. 2D, E), with around half of those increasing the inclusion of the identified splicing events modified by USP10. Next, we wanted to compare the splicing events modified by USP10 with those modified by TDP-43. As we already showed for a couple of targets that USP10 can positively affect the splicing function of TDP-43, we compared the overall splicing changes modified by USP10 overexpression with those affected by TDP-43 overexpression in the same cellular setting. Remarkably, the comparison of the total of the 525 events regulated by USP10 with those modified by TDP-43 overexpression (2500), revealed a clear overlap between the splicing junctions modified by USP10 with a subset of those controlled by TDP-43, with around a quarter of the USP10 controlling splicing events being also modified by TDP-43 (Fig. 2E). To assess the directionality of the changes, we defined the events modified in opposite directions by TDP-43 in our cellular model; for this, we transfected TDP-43 in HeLa cells and compared the RNA-seq obtained from TDP-43 overexpression with downregulation of TDP-43 using an inducible shRNA model in HeLa cells (40). Combining both datasets, we identified around 1650 splice junctions changing in opposite directions between TDP-43 downregulation and overexpression, that we defined as *bona fide* TDP-43 targets in our cellular setting. Focussing on these 1650 targets, we show that around a quarter of these *bona fide* TDP-43 targets move in our USP10 overexpression setting in the same direction as TDP-43 overexpression (Fig. S2D), further supporting a role for USP10 in enhancing TDP-43 splicing function at the transcriptome-wide level. Altogether, these results show for the first time that USP10 can modify alternative splicing, with a clear correlation between some of the splicing events controlled by USP10 and a subset of those controlled by TDP-43.

To assess if USP10 could also enhance TDP-43 splicing function even under TDP-43 loss of function conditions, we turned to our inducible shRNA model in HeLa cells, quantifying the

effects of USP10 overexpression under conditions of TDP-43 loss of function on transcriptome-wide alternative splicing via RNA-seq analysis. We separated the events that increased percentage of exon inclusion (PSI) upon TDP-43 silencing, which included cryptic exons, and those that decreased PSI after TDP-43 downregulation, including skiptic exons (41). Remarkably, USP10 overexpression was able to rescue a proportion of the TDP-43 dependent cryptic, skiptic and cassette exons that changed upon TDP-43 downregulation (Fig. 2F). Importantly, all these changes occurred without significantly affecting *TARDBP* silencing (Fig. S2E). Thus, USP10 can modify the expression of at least a subset of TDP-43 dependent cryptic and skiptic exons, counteracting some of the toxic effects of TDP-43 loss of function.

USP10 is affected in TDP-43 proteinopathies

As TDP-43 proteinopathies are defined at the pathological level by cytoplasmic TDP-43 inclusions, we proceeded to assess USP10 in patient post-mortem material. At the neuropathological level, we performed immunohistochemistry with antibodies against USP10 and phosphorylated TDP-43 (pTDP-43) in paraffin-fixed post-mortem samples from the frontal cortex of FTD patients, separating them by the different types of TDP-43 pathology (FTLD-TDP type A, B or C), which are classified based on the morphology and location of TDP-43 inclusions in the affected cortical areas, and whether they occur in conjunction with ALS (42,43). In agreement with a previous finding from spinal cord of ALS patients (29), we did not find any co-localization between USP10 and pTDP-43 aggregates by immunofluorescence analysis, but we nevertheless verified the presence of the characteristic pTDP-43 staining in all FTLD-TDP pathology subtypes (Fig. 3A). Interestingly, in the frontal cortex of FTLD-TDP type B patients, and to a lesser extent also in FTLD-TDP type A samples, we found increased cytoplasmic immunoreactivity of USP10 in some neurons showing characteristic USP10 staining (Fig. 3B).

Next, we assessed USP10 protein levels by immunoblotting in lysates from ALS and FTD patients cortex, finding a significant increase in USP10 levels in both sets of patients versus controls (Fig. 3C, D). Separating the FTD patients by the type TDP-43 pathology, uncovered a particular increase in USP10 levels on those with FTLD type B TDP-43 pathology, the subtype most commonly associated with ALS, characterised by the presence of TDP-43 positive neuronal cytoplasmic inclusions in all cortical layers (Fig. S3A). Thus, USP10 levels and subcellular localization are altered in the cortex of different TDP-43 proteinopathies.

As USP10 levels increased in TDP-43 proteinopathies patients, we sought to assess the levels of USP10 in different cellular models. We modulated TDP-43 levels by either overexpression or downregulation in different cell lines and assessed possible effects on endogenous USP10 levels at the protein and transcript levels. TDP-43 overexpression did not significantly affect endogenous USP10 levels in HeLa or other cell lines (Fig. S3B). However, acute downregulation of TDP-43 levels by siRNA in HeLa or SH-SY5Y cells led to a significant reduction in endogenous USP10 protein (Fig. 3E and S3C), that was also reflected at the transcript level and was confirmed in the RNA-seq data from HeLa cells with an inducible downregulation of *TARDBP* via shRNA (Fig. S3D). On the other hand, chronic downregulation of *TARDBP* in an inducible human induced pluripotent stem cell i3 model differentiated onto motor neurons (44,45) did not led to any changes in USP10 levels (Fig. S3E). Interestingly, reanalysis of a previously published proteomic dataset obtained from SH-SY5Y cells treated with TDP-43 fibrils that lead to endogenous TDP-43 aggregation (46), showed increased USP10 protein levels in cells with TDP-43 aggregates (Fig. S3F). Overall, these findings imply that, at least in specific contexts, TDP-43 can regulate USP10 levels.

USP10 rescues TDP-43 dependent toxicity *in vivo*

As USP10 was upregulated in ALS and FTD patients, we finally tested the effects of USP10 upregulation on TDP-43 dependent toxicity in an *in vivo* animal model. To assess the effects of TDP-43 toxicity at the whole organism level, we produced a *Drosophila* model overexpressing human TDP-43 in glial cells, leading to major motor deficits associated with decreased survival. In parallel, we developed flies overexpressing human USP10 in glial cells, that did not show any overt motor or survival phenotypes and crossed them with the affected TDP-43 overexpressing strain. Remarkably, human USP10 co-expression with TDP-43 completely rescued the TDP-43 dependent motor deficits in the doubly transgenic flies (Fig. 3F) and potently reduced the associated mortality (Fig. 3G), without significantly affecting human TDP-43 transgene expression levels (Fig. S3G). Thus, USP10 can ameliorate TDP-43 induced toxicity *in vivo*.

DISCUSSION

TDP-43 cytoplasmic aggregation coupled with its nuclear loss are the main pathological hallmarks defining TDP-43 proteinopathies, but how these aggregates are formed and what drives TDP-43 nuclear clearance have not yet been determined. Here, we propose USP10 as a new player in TDP-43 proteinopathies, regulating TDP-43 aggregation and functionality and reducing its toxicity.

Takahashi *et al*. recently described that USP10 promotes the clearance of TDP-43 cytoplasmic aggregates and the formation of TDP-43 aggresomes in cells treated with the proteasome inhibitor MG-132 (29). Some of their results are in contrast with our data, as we did not detect any induction of TDP-43 aggregation mediated by USP10 overexpression. The differences between both studies are likely explained by the different cellular models used, as in their study they mainly focussed on the role of USP10 on TDP-43 aggregation specifically under conditions of proteasome inhibition, which we do not assess here. Interestingly, they

found a direct interaction between TDP-43 and USP10, which we have replicated (data not shown), that is mediated by TDP-43 RNA binding capacity and is likely to play a role in the wider functional connections between TDP-43 and USP10.

Although it is not yet clear how TDP-43 cytoplasmic foci might be formed and their possible relation with SG formation and resolution, we show here that USP10 can indeed modulate TDP-43 cytoplasmic aggregation in all models tested. In all the different paradigms used, USP10 inhibited TDP-43 aggregation irrespective of the cause of aggregation or its possible association with different co-aggregated components, such as whether it colocalizes with SG. This finding is compatible with previous reports proposing that TDP-43 colocalization with SG can be context dependent (47) and that TDP-43 aggregates could occur independent of SG (12). The levels and stoichiometry of G3BP1 and USP10 have been shown to be critical in modulating SG formation (16, 17, 22), with previous data showing that TDP-43 can control *G3BP1* levels through direct mRNA binding (18). Here, we have added another layer of complexity to the role of TDP-43 in modulating SG formation by showing that TDP-43 can, at least in some contexts, regulate USP10 levels. We note that there are multiple published TDP-43 mRNA binding sites in different *USP10* intronic regions (data not shown) that might play a role in this regulation. These findings places TDP-43, USP10 and G3BP1 in a functional hub that together can modulate SG formation, with TDP-43 regulating USP10 and G3BP1 levels, and USP10 in turn controlling TDP-43 levels, functionality and aggregation through a mechanism that requires USP10 interaction with G3BP1.

Moreover, we report that USP10, apart from its wider functions can also modulate transcriptome-wide alternative splicing. Interestingly, we identified a clear overlap between some USP10 modulated exons and a subset of TDP-43 splicing targets, supporting the newly identified functional connection. Further, we show that USP10 can ameliorate the splicing defects due to TDP-43 loss of function without affecting its expression levels (Fig. 2F and

S2E). This, coupled with the inhibiting role of USP10 on TDP-43 aggregation, suggest that USP10 upregulation might be beneficial in TDP-43 proteinopathies by counteracting different aspects of TDP-43 toxicity. To directly test this hypothesis *in vivo*, we generated a *Drosophila* model leading to clear systemic toxicity and motor abnormalities upon TDP-43 overexpression, showing that USP10 upregulation can indeed potently rescue TDP-43 associated phenotypes at the whole organism level (Fig. 3F, G), identifying USP10 as a potential new therapeutic target in TDP-43 proteinopathies.

In patient material, we observed significantly increased USP10 levels in ALS and FTLD patients versus controls (Fig. 3C, D). These results are in contrast with the decrease in USP10 levels that we report in cellular models of acute TDP-43 downregulation (Fig. 3E), or the unaltered USP10 levels in chronic downregulation of *TARDBP* in i3 differentiated motor neurons (Fig. S3E). However, USP10 levels can increase in response to TDP-43 aggregation (Fig. S3F), suggesting that USP10 levels might increase in patients due to the presence of TDP-43 pathology. As our data from different cellular models, together with *Drosophila*, shows that USP10 overexpression could be protective against TDP-43 dependent toxicity, the upregulation seen in some patients might represent a cellular attempt to counteract the toxicity associated with TDP-43 proteinopathy. Moreover, the increase in USP10 levels might inhibit stress granule formation and modulate alternative splicing. Interestingly, recently, USP10 and G3BP1 protein levels have been found to be inversely correlated with TDP-43 pathological burden in postmortem human motor neurons (48), further supporting their functional connection. A number of studies have documented elevated levels of USP10 in other conditions, including glioblastoma and other cancers (49), as well as in Parkinson's disease (PD) affected neurons (50), suggesting that USP10's novel role as a splicing regulator may play a role in the pathophysiology of these disorders. Overall, from all the data presented, further investigations will be required to clarify the complex relation between

TDP-43 and USP10 uncovered here, particularly to clarify the causes and consequences of USP10 upregulation in TDP-43 proteinopathies.

In conclusion, we describe a new functional interaction between USP10 and TDP-43, providing insights into some of the potential molecular mechanisms involved, with both proteins affecting different aspects of the biology of the other, including USP10 modulating TDP-43 aggregation and splicing function, both key molecular mechanisms in TDP-43 proteinopathies. Furthermore, we ascribe a new function to USP10 as a regulator of alternative splicing, with a clear overlap with some TDP-43 splicing targets, further supporting their functional connection. Crucially, we show that USP10 upregulation can rescue TDP-43 dependent toxicity in flies *in vivo*. All these data, together with the finding that USP10 can be altered in ALS and FTD patient material, suggest a possible involvement of USP10 in the pathogenesis of TDP-43 proteinopathies, giving potential clinical relevance to this newly identified functional interaction.

MATERIALS AND METHODS

Cell lines and cultures

All cell lines were cultured at 37^{o} C with 5% CO_2. HeLa, U2OS, Neuro2a were grown in DMEM media (31966, Gibco), whereas SH-SY5Y and SK-N-BE were grown in DMEM/F-12 (50:50), all supplemented with 10% FBS (10082147, Invitrogen) and 1% penicillin/streptomycin (10378016, Invitrogen).

The clover-TDP43$^{\Delta NLS}$ cell line was a kind gift from Don Cleveland (12). The inducible SK-N-BE cell line carrying a doxycycline inducible shRNA against TDP-43 has been published (51). For the induction of *TARDBP* gene silencing, doxycycline (1 µg/ml) (D9891, Sigma) was administered in the culture medium for 3-6 days, depending on the experiment. The

362 inducible Hela cell line carrying the doxycycline inducible shRNA against TDP-43 was
363 generated from a HeLa ATCC clone (CCL-2). Briefly, cells were transduced with an
364 inducible system Tet-pLKO-puro (21915, Addgene) encoding an shRNA targeting *TARDBP*
365 sequence (TRCN0000016038, SIGMA). Lentiviral particles were produced in the HEK293T
366 cell line using psPAX2 (12260, Addgene) and pMD2.G (12259, Addgene) plasmids (both a
367 kind gift from Dr Didier Trono). HeLa cells were transduced and selected with puromycin (1
368 µg/ml) for two weeks. A single clone was isolated and tested for KD efficiency (>80%
369 reduction in protein expression) by doxycycline (200 ng/µl) exposure for three days.

370 iPSC i3LMN: The WTC11 iPSC line derived from a healthy human subject (GM25256) with
371 stable integration of doxycycline-inducible expression of transcription factors NGN2, ISL1,
372 and LHX3 (hNIL) at the CLYBL locus and stable integration of dCas9BFP-KRAB at the
373 CLYBL locus was a gift from Michael Ward (45) and were maintained in E8 Flex Medium
374 (Thermo) in Geltrex (Thermo) coated plates and passed with Versene solution (Thermo) or
375 Accutase (Thermo) when 80% confluent. For induction of iPSCs to i3LMN, iPSCs were
376 passaged with Accutase (Thermo) and plated into Geltrex-coated plates with induction
377 media: DMEM/F12 with Glutamax (Thermo), 1x Non-essential amino acids (Thermo), 2
378 µg/ml doxycycline hyclate (Sigma), 1× N2 supplement (Thermo), and 0,098 µg/ml
379 Compound E (Calbiochem). Media was changed daily for three days. On the second day cells
380 were replated to poly-D-lysine and laminin coated plates. Differentiated neurons were
381 maintained in motor neuron culture media: Neurobasal medium (Gibco) with 1x Non-
382 essential amino acids (Thermo), 1x Glutamax (Thermo), 1x N2 supplement (Thermo), 1x
383 N21 supplement (Thermo), 20 ng/mL BDNF (Peprotech), 20 ng/ml GDNF (Peprotech) 2
384 µg/ml doxycycline hyclate (Sigma), and 1 µg/mL laminin (Thermo) and half media changes
385 were performed twice per week. For the induction of *TARDBP* gene silencing, we use the
386 CRISPRi system (44). The iPSC line was transduced with a lentiviral construct expressing an

sgRNA targeting *TARDBP* gene for 24h, with a subsequent selection by puromycin. Knockdown of *TARDBP* mRNA was robust in iPSCs and in i3LMN for several weeks after differentiation.

Transfections were performed with either jetPRIME (101000046, Polyplus), Lipofectamine 3000 (L3000015, Thermo Fisher) or electroporation with an Amaxa Nucleofector 2b device (AAB-1001, Lonza), all following manufacturer's instructions. For all transfection experiments we used the same amount of DNA for each construct, keeping the total amount of transfected DNA constant with EV. Cells were transfected and harvested after 24 hours, unless otherwise stated.

Cellular stress treatments. To induce TDP-43 cytoplasmic localization and SG in SH-SY5Y, coverslip- plated cells were treated with 500 µM $NaAsO_2$ for 40 minutes, followed by incubation with 600 mM sorbitol for 40 minutes. Cells were then left to recover with fresh media for 1 hour and coverslips processed for microscopy. To induce SG in U2OS cells, 250 µM $NaAsO_2$ was used for 80 minutes. To induce TDP-43 cytoplasmic aggregates in the clover-TDP43$^{\Delta NLS}$ cell line, TDP-43 cytoplasmic localization was induced by doxycycline treatment (1 µg/ml doxycyclin for 24 hours), followed by 250 µM $NaAsO_2$ for 80 minutes.

Small interfering RNAs (siRNAs) specific to human TDP-43 (siTDP43: GCAAAGCCAAGAUGAGCCUTTdTdT), human USP10 (siUSP10: CCCUGAUGGUAUCACUAAAGAdTdT) or negative control luciferase (siLuc: CGUACGCGGAAUACUUCGAUU dTdT), were transfected into U2OS or HeLa cells using Lipofectamine RNAiMAX reagents (Invitrogen) according to the manufacturer's protocol. When a combination of downregulation and overexpression was performed a first round of downregulation was performed on day, followed by a second round on day 2. Then, on day 3, cells were transfected for overexpression using lipofectamine 3000, and harvested on the next day.

412 **Constructs**

413 The GFP-tagged TDP-43-WT and TDP-43$^{\Delta NLS}$ constructs were a kind gift from the
414 laboratory of Leonard Petrucelli (52). The CFTR C155T TG11T5 minigene was a kind gift
415 from Emanuele Buratti (53,54). The USP10 WT and USP10^{C424A} construct were kindly
416 provided by Lorenza Penengo (University of Zurich, Switzerland). The USP10^{F10A} mutant
417 was made using site directed mutagenesis following manufacturer's instructions (Agilent).
418 All constructs were amplified in commercial *E. coli* lines and plasmids purified (740410.50,
419 Macherey Nagel) according to the manufacturer's instructions.

420 **Antibodies**

421 The following antibodies and concentrations were used for immunoblot and
422 immunofluorescence staining:
423 Rabbit anti TDP-43 (WB 1:1000, IF 1:400, Protein Tech, 10782-2-AP); mouse anti TDP-43
424 (WB 1:5000, abcam, ab104223); mouse anti TDP-43 (IF 1:200, R&D systems, MAB37778);
425 mouse anti pTDP-43 (IF 1:3000, Cosmobio, CAC-TIP-PTD-M01); mouse anti G3BP1 (IF
426 1:300, Protein Tech, 66486-1-Ig); rabbit anti G3BP1 (WB: 1:2000, IF 1:300, Protein Tech,
427 13057-2-AP); rabbit anti G3BP2 (IF 1:300, Protein Tech, 16276-1-AP); rabbit anti USP10
428 (WB 1:1000, IF 1:500, Sigma-Aldrich, HPA006731); rabbit anti USP10 (WB 1:1000, made
429 in house from the Freire laboratory); rabbit anti USP10 (IF 1:200, Bethyl, A300-901A);
430 mouse anti Tubulin (WB 1:10000, Protein Tech, 11224-1-AP); mouse anti β-Tubulin
431 (WB 1:10000, Protein Tech, 66240-1-Ig); mouse anti GAPDH (WB 1:250, Santa
432 Cruz Biotechnology, sc-32233); anti mouse Alexa Fluor 488 (IF secondary 1:600, Thermo
433 Fisher, Z25002); anti rabbit Alexa Fluor 488 (IF secondary 1:600, Thermo Fisher, Z25302);
434 anti mouse Alexa Fluor 568 (IF secondary 1:600, Thermo Fisher, Z25006); anti rabbit Alexa
435 Fluor 568 (IF secondary 1:600, Thermo Fisher, Z25306). The antibody against human USP10
436 was generated by injecting rabbits with a His-tagged antigen (amino acids 1-350). The

antigen was obtained by cloning the corresponding cDNA in pET-30 (Novagen), followed by expression in E. coli and purification with a Ni-NTA resin (Qiagen) following manufacturers recommendations.

Patient material

We obtained frontal cortex brain tissue from the UCL Queen Square Brain Bank, separated FTLD cases according to the subtype of TDP-43 pathology and a control group of deceased patients with no pathologies described. Lysates from ALS motor cortex and controls came from the Bellvitge Hospital (Barcelona). All biological samples comply with the legal requirements of consent, collection, use and storage.

Immunofluorescence

Cells were grown in plates containing sterile glass coverslips, fixed with 4 % PFA (P6148, Sigma-Aldrich), permeabilised using 0.5% Triton detergent (85111, Thermo Fisher) and blocked with BSA (422381B, VWR). The samples were then incubated overnight with primary antibodies in BSA, and then with appropriate secondary antibodies. Slides were mounted using ProLong™ (P36962, Thermo Fisher) and samples visualised on a Zeiss Axio Observer fluorescence microscope, with images analysed using Image J software 50.

The immunohistochemistry experiments from patient material were carried out on 20 µm thick paraffin-embedded sections obtained from the Queen Square Brain Bank for Neurological Disorders (University College of London). Antigenic unmasking was performed using the Dako PT Link PT100 Slide Stainer (Swerdlick Medical Systems), prior to permeabilization with 0.5% Triton. Immunofluorescence or DAB was used for visualized (15454629, Thermo Fisher) using a Leica DMi1 light microscope.

For the detection and quantification of TDP-43-positive aggregates and SG, pictures of 50-100 cells from random fields were taken with a Zeiss Axio Observer fluorescence

461 microscope, and the images taken analysed using Image J software. Aggregates were
462 analysed with the Aggrecount (55) Image J plugin. The data collected were the number of
463 aggregates per cell, the number of cells with aggregates and the size of the aggregates. To
464 consider that a cell had TDP-43 inclusions or SG, cells with more than two TDP-43
465 inclusions/SG larger than 0.5-1 μm^2 were taken as positive. For colocalization studies, a line
466 profile analysis was performed and the quantification was done using JaCoP in Image J
467 giving the Pearson coefficient and the mass centre coincidence (56).

468 **Protein extractions**

469 From cell lines, proteins were extracted by resuspending cells from 6-well plates in 100 µl of
470 RIPA or 7M Urea Buffer containing protease inhibitor (11873580001, Roche) and, if
471 necessary, phosphatase inhibitor (04906837001, Roche). Cell lysates were centrifuged at >14
472 000 x g for 15 minutes, discarding the sediment. Supernatant was then sonicated using an
473 ultrasonic homogeniser (UP50H, Hielscher) for 15 seconds. Protein concentration in the
474 soluble extract was quantified by using the BCA method (Thermo Scientific). For post-
475 mortem material from FTD patients, 13mg of frozen sample was weighed, to which 0.26 ml
476 of 7M Urea buffer was added and homogenised using a rotary homogeniser (BK-HG,
477 Biobase). The samples were then sonicated using an ultrasonic homogeniser (UP50H,
478 Hielscher) for 15 seconds. Samples were frozen at -80°C until use.

479 **Immunoblots**

480 Cell lysates were resuspended in Laemmli buffer and heated at 95°C for 5 minutes. Then,
481 proteins were separated by 10% SDS polyacrylamide gel electrophoresis (SDS-PAGE) using
482 a Mini-PROTEAN kit (1658001FC, Bio-Rad). Between 20 and 50 µg of protein per well
483 was loaded. After the separation, proteins were transferred onto a nitrocellulose (1620115,
484 BioRad) or PVDF (1620177, Bio-Rad) membrane, that was blocked with either BSA or milk
485 powder. The primary antibodies and concentrations used are listed in the antibodies section.

Bands were detected via ECL (1705060, Bio-Rad), viewed on a ImageQuant™ LAS 4000 chemiluminescence reader (GE Healthcare), and analysed by densitometry using the Image Quant TL software.

RNA isolation, RT–PCR and qPCR

RNA extractions were carried out using TRIzol (15596-026, Invitrogen), according to manufacturer's instructions. For complementary DNA synthesis, the qScript cDNA synthesis kit (95047, QuantaBio) was used, using as a template 100-500 ng of RNA. RT-PCR for splicing events was conducted using 2X PCR Master Mix (11816843, Thermo Fisher) with specific primers (see below) spanning the differentially expressed exon. Products were electrophoresed on 2.5% agarose gels containing ethidium bromide and visualized on an automated image detection system (Gel Doc EZ, BioRad). The BioRad Image Lab software was used to quantify the bands. Results were analysed using the percentage of exclusion (PSE), calculated dividing the intensity of the shorter exon exclusion band by the sum of both exon inclusion and exon exclusion bands. Primers used here were:

RABGEF exon 16: CTGCAGACAAAGCACACACGAT and

GCACAGAGGAGATCCGATTGAT

RWDD1 exon 2: GGGCCACGATGACAGATTAC and AGGAGGGTTGGATCAATGTG

CFTR minigene: CAACTTCAAGCTCCTAAGCCACTGC and

TAGGATCCGGTCACCAGGAAGTTGGTTAAATCA

qPCR was used to quantify mRNA expression using specific primers (see below). SYBR Green (PB20.11-05, PCR Biosystems) was used on a real-time thermal cycler (LightCycler® 480, Roche). *S16* or *HPRT* were used as internal control gene. The levels of messenger RNA were assessed by calculating ΔΔCT which shows the relative expression change (fold change), normalised to the housekeeping gene. For all samples analysed, 3 technical replicates and 3 biological replicates were performed. The primers:

GFP: AAGCAGAAGAACGGCATCAAG and TCAGGTAGTGGTTGTCGGGCA

USP10: GGGTGCCAGAAGCTTATCAA and CACTGTTGCCGTGATGGTAG

TARDBP (exon 1-2): CTGCTTCGGTGTCCCTGT and ATGGGCTCATCGTTCTCATC

TARDBP (exon 5-6): ATGACTGAGGATGAGCTGCG and

CACAAAGAGACTGCGCAATCT

S16: AAGTCTTCGGACGCAAGAAA and TGCCCAGAAGCAGAACAG

HPRT: TTTGCTGACCTGCTGCTGGATTAC and TTGACCATCTTTGGATTATACTGC

RNA sequencing analysis

RNA was quality checked using a Tapestation (Agilent) prior to submission to the UCL Genomics facility; sequencing libraries were prepared with polyA enrichment and sequenced with 150 nt paired reads.

Raw sequences (in fastq format) were trimmed using Fastp with the parameter "qualified_quality_phred: 10", and aligned using STAR (v2.7.0f) to the Grch38 with gene models from GENCODE v40 (57–59).

The STAR outputs are BAM files, containing the counts and coordinates for all splice junctions found in the sample, and alignment metadata including the genomic location where a read is mapped to, read sequence, and quality score. Then, using samtools, BAM files were sorted and indexed by the read coordinates location (60).

Trimmed fastqc files were aligned to the transcriptome using Salmon (v1.5.1), outputting isoform-specific counts used for differential gene expression, performed using DeSEQ2 without covariates, using an index built from GENCODE v40 (61,62). The DESeq2 median of ratios, which controls for both sequencing depth and RNA composition, was used to normalise gene counts. Differential expression was defined at a Benjamini–Hochberg false discovery rate < 0.1. We kept genes with at least 5 counts per million in more than 2 samples.

Splicing analysis was performed using Majiq (v2.1) on STAR-aligned and sorted BAMs and the Grch38 reference genomes. Cryptic splicing was defined as junctions with Ψ (PSI, percent spliced in) < 5% in the control samples and ΔΨ > 10% between groups, while skiptic splicing as junctions with Ψ > 95% in the control samples and ΔΨ < - 10% between groups. Other junctions were classified as differentially spliced when the absolute value of ΔΨ was above 10% between groups.

The alignment and splicing pipelines are implemented in Snakemake (v5.5.4), a workflow management software that allows reliable, reproducible, and scalable analysis, and run on the UCL high-performance cluster (HPC) (63). DESeq2 and data visualisation were run using R with the packages tidyverse, rstatix, and eulerr, and custom scripts available upon request.

USP10 analysis from published datasets

The mass spectrometry proteomics data from Scialò C et al (46), was downloaded from the ProteomeXchange Consortium repository (64) under the dataset identifier PXD058981. From the report.tsv file generated by DIA-NN, which contains precursor ion abundances for each raw file, protein abundances were obtained by first aggregating precursor abundances to peptidoform abundances, followed by estimation via Tukey's median polish using the R package prolfqua (65). Protein abundances were transformed using robscale prior to fitting linear models, and expressed relative to negative controls, which were set to a value of 1. Data are shown as mean with s.d. as indicated in the figure legends. Statistical significance was assessed by t-test.

The RNA-sequencing data from Scialò C et al (46), have been downloaded from GEO database (66) under accession number GSE285224. The normalized counts were expressed relative to negative controls, which were set to a value of 1. Data are shown as mean with s.d. as indicated in the figure legends. Statistical significance was assessed by t-test.

559 ***Drosophila* models**

560 Different *Drosophila* strains were obtained from Vienna Stock Center (VDRC, Austria) and
561 Bloomington Stock Centre (BDSC, Indiana-USA). REPO was used as the driver for
562 conditional expression in glial cells (BDSC, #7415), that was crossed with strains carrying
563 sequences to express human TDP-43 (BDSC, #79587) and USP10, the later one was newly
564 generated using Bestgene Inc. via their embryo injection service, with the strain selected
565 expressing the highest amount of USP10 measured by RT-PCR.

566 The analysed experimental genotypes for glial expression were (G-E)-(UAS-
567 hTDP43///REPO-Gal4) and (G-E)-(UAS-hUSP10///REPO-Gal4). Stocking flies were housed
568 at 22□°C, 70% humidity and 12□h/12□h light/darkness cycle and experimental flies at 26
569 °C, 70% humidity and 12□h/12□h light/darkness cycle.

570 *Drosophila functional assays.* For longevity tests, 50 adult female flies (five per tube) were
571 selected from each strain. Dead flies were counted every 2 days and tubes were replaced
572 every 7 days. Mantel-Cox method was used to analyse the results. For locomotor activity,
573 adult flies were tested on day 7 in groups of five (the same groups as in the longevity test).
574 They were placed in a tube with a line drawn outside the tube at a height of 8 cm from the
575 bottom. The number of flies crossing the line in 10s was counted (3 trials per tube). The
576 results were analysed using t-student analysis. Adult pharate survival was expressed as a
577 percentage of adult flies counted over the total number of pupae in each tube, where adult
578 pharate survival of control flies were approximately 100%.

579 *Drosohila RNA extraction and quantitative real time PCR.* Total RNA was extracted from 2-
580 4 independent experimental pools using the RNeasy Mini Kit (ref. 74104, QIAGEN). Each
581 pool consisted of 10 thoraces, 20 brains or 30 ventral nerve cords (VNCs), depending on the
582 tissue to be analysed. Reverse transcription was performed using the SuperScript VILO
583 cDNA Synthesis Kit (Thermo Fisher) according to the manufacturer instructions.

Quantitative real-time PCR was performed on a CFX384 Touch Real-Time PCR Detection System (Bio-Rad) using Powe SYBR Green Master Mix (Thermo Fisher), 300 nM of primer pair, and 10 ng of cDNA. Tubulin (Tub) was used as a housekeeping gene. The 2-ΔΔCt method was used for relative quantification. The primers sequences used for genotype confirmation were pre-designed and obtained from Sigma-Aldrich: Tbph - DMEL_TBPH_8, TARDBP – H_TARDBP_1.

Statistics

Results were analysed using GraphPad Prism 8.0.2 software. Data are generally presented as the mean accompanied by the standard error (Mean±SEM). Test and sample sizes used are generally specified in each figure. For parametric samples, t-test and/or ANOVA was performed. For non-parametric samples, the Mann-Whitney U test or Kluskal Wallis were used. Statistical significance is attributed at a p value <0.05.

Funding

This research was funded by grants to AA-A by the Instituto de Salud Carlos III (ISCIII: PI17/00244 and PI20/00422), grant PID2023-147267OB-I00 funded by MCIN/AEI/10.13039/501100011033 and ERDF/EU as well as CIBERNED. AA-A was funded by a Miguel Servet fellowship and LTG by a Sara Borrell fellowship both from the ISCIII; JMBA is funded by CIBERNED; FF is funded by a Juan de la Cierva *formacion* fellowship FJC2021-046836-I financed by MICIU/AEI/10.13039/501100011033 and the EU NextGeneration. RMBA is co-funded by ACIISI of the *Consejería de Economía, Industria, Comercio y Conocimiento and Fondo Social Europeo*.

Acknowledgements

We thank Professor Elizabeth MC Fisher for critical reading of the manuscript. We are grateful to Professors Don Cleveland, Leonard Petrucelli, Sandrine Da Cruz, Michael Ward and Lorenza Penengo for sharing critical reagents.

Conflict of interests

The authors declare that they have no conflict of interest.

FIGURE LEGENDS

Figure 1. TDP-43 cytoplasmic aggregation is modulated by USP10 through its interaction with G3BP1. (A) Representative fluorescence images showing GFP_TDP-43 aggregates in HeLa cells 24 hours after co-transfection with GFP_TDP-43$^{\Delta NLS}$ and USP10 or an EV, co-labelled with anti-G3BP1 primary antibody in red marking SG. Scale bar: 10 µm. Quantification of the percentage of cells with more than two GFP_TDP-43$^{\Delta NLS}$ aggregates bigger than 1 µm; the average size of the TDP-43 aggregates; the percentage of cells with more than two SG bigger than 0.5 µm; and the average size of SG, comparing in all panels GFP_TDP-43$^{\Delta NLS}$ cotransfection with an EV (NLS group) with the co-transfection of GFP_TDP-43$^{\Delta NLS}$ and USP10 (NLS + USP10). For all figure panels, each datapoint corresponds to one independent experiment on which at least 50 cells per group were analysed. *p<0.05, **p<0.01, ***p<0.001 analysed by Mann-Whitney U test, with error bars showing the SEM for all panels. **(B)** Representative fluorescence images showing TDP-43 aggregates in green and SG labelled with G3BP1 in red, in U2OS cells 24 hours after endogenous Clover_TDP-43$^{\Delta NLS}$ induction with doxycycline and transfection with an EV or USP10 followed by induction of TDP-43 aggregation with 250 µM $NaAsO_2$ for 80 minutes. Scale bar: 10 µm. Quantification of the average size and percentage of cells with more than two Clover_TDP-43 aggregates bigger than 0.5 µm after transfection with USP10 or EV, together with the size and percentage of cells with SG bigger than 0.5 µm. **(C)** Representative images of TDP-43 aggregates (green) in HeLa cells 24 hours after co- transfection with GFP_TDP-43$^{\Delta NLS}$ and either an EV, USP10^{WT}, USP10^{F10A} or USP10^{C424A}. Scale bar: 10 µm. **(D)** Representative images of TDP-43 aggregates (green) in doxycycline inducible TDP-43$^{\Delta NLS}$ U2OS cells 24 hours after doxycycline and 80 minutes after $NaAsO_2$ (250 µM) treatment. Cells were transfected with either an EV, USP10^{WT}, USP10^{F10A} or USP10^{C424A}. Scale bar: 10 µm.

Figure 2. USP10 regulates alternative splicing and enhance TDP-43 splicing function. **(A)** Representative image and quantification of the PSE (percentage of splicing exclusion) of the *CFTR* exon 9 minigene. HeLa cells were cotransfected with the *CFTR* minigene and either EV or USP10. Following RT-PCR, the PSE was quantified by densitometry, comparing to the EV via one-way ANOVA. For all figure panels, each data point represents a different cellular well, with the different shapes representing independent experiments. *p<0.05, **p<0.01, ***p<0.001 and error bars represent SEM for all figure panels. **(B)** Representative image and quantification of the PSE of *RABGEF* exon 16. HeLa cells were transfected with either an EV or USP10. Following RT-PCR, the PSE was quantified and compared via one-way ANOVA. **(C)** Representative image of immunoblots in U2OS cells treated with siRNA against *USP10* (siUSP10) or siRNA against luciferase (siControl). TDP-43 levels were quantified via densitometry, using GAPDH as loading control, displaying the ratio of the siControl group as 100%. *p<0.05, by Mann-Whitney U-test. N=13, from 3 independent experiments. And quantification of the relative ΔΔCt expression levels of *TARDBP* transcript with *HPRT* control does not show a significant difference after USP10 downregulation when compared to siControl by Mann-Whitney U-test (p=0.3). N=10, from 3 independent experiments. (**D**) Sahimi plot examples of splicing events modified by USP10 overexpression. Top: *PKD1P4* skipping of exon 6. Bottom: *DAB2IP* splice site inside exon 11. **(E)** Venn diagram showing the overlap between splicing events shared between USP10 and TDP-43 overexpression. **(F)** Representation of the changes in the PSI of skiptic exons (bottom) and cryptic exons (top) that are rescued (green) or not (grey) by the overexpression of USP10 after TDP-43 downregulation in HeLa cells. A subset of the most changed splicing events is also annotated with the gene name.

Figure 3. **USP10 is affected in TDP-43 proteinopathies and can ameliorate TDP-43 toxicity *in vivo*.** **(A)** Representative immunofluorescence and **(B)** immunohistochemistry

images of post-mortem slices of frontal cortex samples from FTD patients. In (A), primary anti-pTDP-43 labelled in green, anti-USP10 in red, and nuclei in blue (DAPI), showing the merged images from the three channels. In (B) primary anti-USP10 revealed with DAB. Red arrows show increased USP10 immunoreactivity in the cytoplasm of some neurons. Scale bars: 50 μm. **(C)** Representative image of immunoblot and quantification of USP10 in protein lysates of motor cortex from 5 ALS patients and 5 controls and **(D)** frontal cortex from FTD 6 patients and 3 controls. For both panels, USP10 bands were quantified by densitometry, using β-Tubulin as loading control, normalizing to the average of each of the control groups (100%), displaying the percentage of the USP10/β-Tubulin ratio and comparing by Mann-Whitney U-test. (**E**) Representative image of immunoblot and quantification of SH-SY5Y downregulated for 72 h with either siRNA against *TARDBP* or a negative control (siControl). Quantification of USP10 bands by densitometry was normalized to their loading control (β-Tubulin). The quantification shown corresponds to a N=3, from one experiment, corroborated by another independent experiment, compared by T test to control. **(F)** *Drosophila* locomotor activity for the selected genotypes tested on day 7, quantified by the ability to climb an 8 cm mark inside a tube, normalised by the performance of the control group (100%), compared by Kruskal Wallis test. **(G)** Percentage of survival of the selected *Drosophila* genotypes of 50 adult female flies for each strain compared by Mantel-Cox. *< 0.05; **p<0,01 and ***p<0,001, with error bars show SEM for all figure panels.

685 # REFERENCES

686

687 1. Taylor JP, Brown RH, Cleveland DW. Decoding ALS: from genes to mechanism. Nature. 2016 Nov
688 10;539(7628):197–206.

689 2. Strong MJ, Abrahams S, Goldstein LH, Woolley S, Mclaughlin P, Snowden J, et al. Amyotrophic
690 lateral sclerosis - frontotemporal spectrum disorder (ALS-FTSD): Revised diagnostic criteria.
691 Amyotroph Lateral Scler Front Degener. 2017 Apr 3;18(3–4):153–74.

692 3. Ling SC, Polymenidou M, Cleveland DW. Converging Mechanisms in ALS and FTD: Disrupted RNA
693 and Protein Homeostasis. Neuron. 2013 Aug;79(3):416–38.

694 4. Coyne AN, Zaepfel BL, Zarnescu DC. Failure to Deliver and Translate—New Insights into RNA
695 Dysregulation in ALS. Front Cell Neurosci. 2017 Aug 17;11:243.

696 5. Buratti E. Trends in Understanding the Pathological Roles of TDP-43 and FUS Proteins. In: Ghetti
697 B, Buratti E, Boeve B, Rademakers R, editors. Frontotemporal Dementias [Internet]. Cham:
698 Springer International Publishing; 2021 [cited 2024 Jan 19]. p. 243–67. (Advances in
699 Experimental Medicine and Biology; vol. 1281). Available from:
700 https://link.springer.com/10.1007/978-3-030-51140-1_15

701 6. Neumann M, Sampathu DM, Kwong LK, Truax AC, Micsenyi MC, Chou TT, et al. Ubiquitinated
702 TDP-43 in Frontotemporal Lobar Degeneration and Amyotrophic Lateral Sclerosis. Science. 2006
703 Oct 6;314(5796):130–3.

704 7. Nelson PT, Dickson DW, Trojanowski JQ, Jack CR, Boyle PA, Arfanakis K, et al. Limbic-
705 predominant age-related TDP-43 encephalopathy (LATE): consensus working group report.
706 Brain. 2019 June 1;142(6):1503–27.

707 8. Mehta PR, Brown AL, Ward ME, Fratta P. The era of cryptic exons: implications for ALS-FTD. Mol
708 Neurodegener. 2023 Mar 15;18(1):16.

709 9. Vanden Broeck L, Kleinberger G, Chapuis J, Gistelinck M, Amouyel P, Van Broeckhoven C, et al.
710 Functional complementation in Drosophila to predict the pathogenicity of TARDBP variants:
711 evidence for a loss-of-function mechanism. Neurobiol Aging. 2015 Feb;36(2):1121–9.

712 10. Ederle H, Dormann D. TDP -43 and FUS *en route* from the nucleus to the cytoplasm. FEBS Lett.
713 2017 June;591(11):1489–507.

714 11. Cook C, Petrucelli L. Genetic Convergence Brings Clarity to the Enigmatic Red Line in ALS.
715 Neuron. 2019 Mar;101(6):1057–69.

716 12. Gasset-Rosa F, Lu S, Yu H, Chen C, Melamed Z, Guo L, et al. Cytoplasmic TDP-43 De-mixing
717 Independent of Stress Granules Drives Inhibition of Nuclear Import, Loss of Nuclear TDP-43, and
718 Cell Death. Neuron. 2019 Apr;102(2):339-357.e7.

719 13. Ivanov P, Kedersha N, Anderson P. Stress Granules and Processing Bodies in Translational
720 Control. Cold Spring Harb Perspect Biol. 2019 May;11(5):a032813.

14. Wolozin B, Ivanov P. Stress granules and neurodegeneration. Nat Rev Neurosci. 2019 Nov;20(11):649–66.

15. Advani VM, Ivanov P. Stress granule subtypes: an emerging link to neurodegeneration. Cell Mol Life Sci. 2020 Dec;77(23):4827–45.

16. Kedersha N, Panas MD, Achorn CA, Lyons S, Tisdale S, Hickman T, et al. G3BP–Caprin1–USP10 complexes mediate stress granule condensation and associate with 40S subunits. J Cell Biol. 2016 Mar 28;212(7):e201508028.

17. Yang P, Mathieu C, Kolaitis RM, Zhang P, Messing J, Yurtsever U, et al. G3BP1 Is a Tunable Switch that Triggers Phase Separation to Assemble Stress Granules. Cell. 2020 Apr;181(2):325-345.e28.

18. McDonald KK, Aulas A, Destroismaisons L, Pickles S, Beleac E, Camu W, et al. TAR DNA-binding protein 43 (TDP-43) regulates stress granule dynamics via differential regulation of G3BP and TIA-1. Hum Mol Genet. 2011 Apr 1;20(7):1400–10.

19. Aulas A, Stabile S, Vande Velde C. Endogenous TDP-43, but not FUS, contributes to stress granule assembly via G3BP. Mol Neurodegener. 2012 Dec;7(1):1.

20. Aulas A, Vande Velde C. Alterations in stress granule dynamics driven by TDP-43 and FUS: a link to pathological inclusions in ALS? Front Cell Neurosci [Internet]. 2015 Oct 23 [cited 2024 Jan 19];9. Available from: http://journal.frontiersin.org/Article/10.3389/fncel.2015.00423/abstract

21. Sidibé H, Khalfallah Y, Xiao S, Gómez NB, Fakim H, Tank EMH, et al. TDP-43 stabilizes G3BP1 mRNA: relevance to amyotrophic lateral sclerosis/frontotemporal dementia. Brain J Neurol. 2021 Dec 16;144(11):3461–76.

22. Panas MD, Schulte T, Thaa B, Sandalova T, Kedersha N, Achour A, et al. Viral and Cellular Proteins Containing FGDF Motifs Bind G3BP to Block Stress Granule Formation. Heise MT, editor. PLOS Pathog. 2015 Feb 6;11(2):e1004659.

23. Sanders DW. Competing Protein-RNA Interaction Networks Control Multiphase Intracellular Organization. Cell. 2020;181:306–24.

24. Sheehan CT, Hampton TH, Madden DR. Tryptophan mutations in G3BP1 tune the stability of a cellular signaling hub by weakening transient interactions with Caprin1 and USP10. J Biol Chem. 2022 Dec;298(12):102552.

25. Yuan J, Luo K, Zhang L, Cheville JC, Lou Z. USP10 Regulates p53 Localization and Stability by Deubiquitinating p53. Cell. 2010 Feb;140(3):384–96.

26. Meyer C, Garzia A, Morozov P, Molina H, Tuschl T. The G3BP1-Family-USP10 Deubiquitinase Complex Rescues Ubiquitinated 40S Subunits of Ribosomes Stalled in Translation from Lysosomal Degradation. Mol Cell. 2020 Mar;77(6):1193-1205.e5.

27. Garshott DM, An H, Sundaramoorthy E, Leonard M, Vicary A, Harper JW, et al. iRQC, a surveillance pathway for 40S ribosomal quality control during mRNA translation initiation. Cell Rep. 2021 Aug;36(9):109642.

28. Piatnitskaia S, Takahashi M, Kitaura H, Katsuragi Y, Kakihana T, Zhang L, et al. USP10 is a critical factor for Tau-positive stress granule formation in neuronal cells. Sci Rep. 2019 Dec;9(1):10591.

29. Takahashi M, Kitaura H, Kakita A, Kakihana T, Katsuragi Y, Onodera O, et al. USP10 inhibits aberrant cytoplasmic aggregation of TDP-43 by promoting stress granule clearance. Mol Cell Biol. 2022 Jan 10;MCB.00393-21.

30. Lee KH, Zhang P, Kim HJ, Mitrea DM, Sarkar M, Freibaum BD, et al. C9orf72 Dipeptide Repeats Impair the Assembly, Dynamics, and Function of Membrane-Less Organelles. Cell. 2016 Oct;167(3):774-788.e17.

31. Zhang YJ, Caulfield T, Xu YF, Gendron TF, Hubbard J, Stetler C, et al. The dual functions of the extreme N-terminus of TDP-43 in regulating its biological activity and inclusion formation. Hum Mol Genet. 2013 Aug 1;22(15):3112–22.

32. Markmiller S, Soltanieh S, Server KL, Mak R, Jin W, Fang MY, et al. Context-Dependent and Disease-Specific Diversity in Protein Interactions within Stress Granules. Cell. 2018 Jan;172(3):590-604.e13.

33. Fang MY, Markmiller S, Vu AQ, Javaherian A, Dowdle WE, Jolivet P, et al. Small-Molecule Modulation of TDP-43 Recruitment to Stress Granules Prevents Persistent TDP-43 Accumulation in ALS/FTD. Neuron. 2019 Sept;103(5):802-819.e11.

34. Pickart CM. Mechanisms Underlying Ubiquitination. Annu Rev Biochem. 2001 June;70(1):503–33.

35. Clague MJ, Barsukov I, Coulson JM, Liu H, Rigden DJ, Urbé S. Deubiquitylases From Genes to Organism. Physiol Rev. 2013 July;93(3):1289–315.

36. Liu J, Xia H, Kim M, Xu L, Li Y, Zhang L, et al. Beclin1 Controls the Levels of p53 by Regulating the Deubiquitination Activity of USP10 and USP13. Cell. 2011 Sept;147(1):223–34.

37. Bomberger JM, Barnaby RL, Stanton BA. The Deubiquitinating Enzyme USP10 Regulates the Post-endocytic Sorting of Cystic Fibrosis Transmembrane Conductance Regulator in Airway Epithelial Cells. J Biol Chem. 2009 July;284(28):18778–89.

38. He Y, Jiang S, Mao C, Zheng H, Cao B, Zhang Z, et al. The deubiquitinase USP10 restores PTEN activity and inhibits non–small cell lung cancer cell proliferation. J Biol Chem. 2021 Sept;297(3):101088.

39. Buratti E, Baralle FE. Characterization and Functional Implications of the RNA Binding Properties of Nuclear Factor TDP-43, a Novel Splicing Regulator ofCFTR Exon 9. J Biol Chem. 2001 Sept;276(39):36337–43.

40. Ceron-Codorniu M, Torres P, Fernàndez-Bernal A, Rico-Rios S, Serrano JC, Miralles MP, et al. TDP-43 dysfunction leads to bioenergetic failure and lipid metabolic rewiring in human cells. Redox Biol. 2024 Sept;75:103301.

41. Fratta P, Sivakumar P, Humphrey J, Lo K, Ricketts T, Oliveira H, et al. Mice with endogenous TDP -43 mutations exhibit gain of splicing function and characteristics of amyotrophic lateral sclerosis. EMBO J. 2018 June;37(11):e98684.

42. Lashley T, Rohrer JD, Mead S, Revesz T. Review: an update on clinical, genetic and pathological aspects of frontotemporal lobar degenerations. Neuropathol Appl Neurobiol. 2015 Dec;41(7):858–81.

43. Laferrière F, Maniecka Z, Pérez-Berlanga M, Hruska-Plochan M, Gilhespy L, Hock EM, et al. TDP-43 extracted from frontotemporal lobar degeneration subject brains displays distinct aggregate assemblies and neurotoxic effects reflecting disease progression rates. Nat Neurosci. 2019 Jan;22(1):65–77.

44. Tian R, Gachechiladze MA, Ludwig CH, Laurie MT, Hong JY, Nathaniel D, et al. CRISPR Interference-Based Platform for Multimodal Genetic Screens in Human iPSC-Derived Neurons. Neuron. 2019 Oct 23;104(2):239-255.e12.

45. Fernandopulle MS, Prestil R, Grunseich C, Wang C, Gan L, Ward ME. Transcription Factor-Mediated Differentiation of Human iPSCs into Neurons. Curr Protoc Cell Biol. 2018 June;79(1):e51.

46. Scialò C, Zhong W, Jagannath S, Wilkins O, Caredio D, Hruska-Plochan M, et al. Seeded aggregation of TDP-43 induces its loss of function and reveals early pathological signatures. Neuron. 2025 May 21;113(10):1614-1628.e11.

47. Dewey CM, Cenik B, Sephton CF, Johnson BA, Herz J, Yu G. TDP-43 aggregation in neurodegeneration: Are stress granules the key? Brain Res. 2012 June;1462:16–25.

48. Guise AJ, Misal SA, Carson R, Chu JH, Boekweg H, Van Der Watt D, et al. TDP-43-stratified single-cell proteomics of postmortem human spinal motor neurons reveals protein dynamics in amyotrophic lateral sclerosis. Cell Rep. 2024 Jan;43(1):113636.

49. Grunda JM, Nabors LB, Palmer CA, Chhieng DC, Steg A, Mikkelsen T, et al. Increased Expression of Thymidylate Synthetase (TS), Ubiquitin Specific Protease 10 (USP10) and Survivin is Associated with Poor Survival in Glioblastoma Multiforme (GBM). J Neurooncol. 2006 Nov 9;80(3):261–74.

50. Takahashi M, Kitaura H, Kakita A, Kakihana T, Katsuragi Y, Nameta M, et al. USP10 Is a Driver of Ubiquitinated Protein Aggregation and Aggresome Formation to Inhibit Apoptosis. iScience. 2018 Nov;9:433–50.

51. Brown AL, Wilkins OG, Keuss MJ, Hill SE, Zanovello M, Lee WC, et al. TDP-43 loss and ALS-risk SNPs drive mis-splicing and depletion of UNC13A. Nature. 2022 Mar;603(7899):131–7.

52. Wang W, Li L, Lin WL, Dickson DW, Petrucelli L, Zhang T, et al. The ALS disease-associated mutant TDP-43 impairs mitochondrial dynamics and function in motor neurons. Hum Mol Genet. 2013 Dec 1;22(23):4706–19.

53. Pagani F, Buratti E, Stuani C, Baralle FE. Missense, Nonsense, and Neutral Mutations Define Juxtaposed Regulatory Elements of Splicing in Cystic Fibrosis Transmembrane Regulator Exon 9. J Biol Chem. 2003 July;278(29):26580–8.

54. D'Ambrogio A, Buratti E, Stuani C, Guarnaccia C, Romano M, Ayala YM, et al. Functional mapping of the interaction between TDP-43 and hnRNP A2 in vivo. Nucleic Acids Res. 2009 July 1;37(12):4116–26.

55. Klickstein JA, Mukkavalli S, Raman M. AggreCount: An unbiased image analysis tool for identifying and quantifying cellular aggregates in a spatially-defined manner. J Biol Chem. 2020 Oct 20;jbc.RA120.015398.

837 56. Bolte S, Cordelières FP. A guided tour into subcellular colocalization analysis in light microscopy.
838 J Microsc. 2006 Dec;224(3):213–32.

839 57. Chen S, Zhou Y, Chen Y, Gu J. fastp: an ultra-fast all-in-one FASTQ preprocessor. Bioinformatics.
840 2018 Sept 1;34(17):i884–90.

841 58. Dobin A, Davis CA, Schlesinger F, Drenkow J, Zaleski C, Jha S, et al. STAR: ultrafast universal RNA-
842 seq aligner. Bioinformatics. 2013 Jan 1;29(1):15–21.

843 59. Frankish A, Diekhans M, Ferreira AM, Johnson R, Jungreis I, Loveland J, et al. GENCODE
844 reference annotation for the human and mouse genomes. Nucleic Acids Res. 2019 Jan
845 8;47(D1):D766–73.

846 60. Li H, Handsaker B, Wysoker A, Fennell T, Ruan J, Homer N, et al. The Sequence Alignment/Map
847 format and SAMtools. Bioinformatics. 2009 Aug 15;25(16):2078–9.

848 61. Patro R, Duggal G, Love MI, Irizarry RA, Kingsford C. Salmon provides fast and bias-aware
849 quantification of transcript expression. Nat Methods. 2017 Apr;14(4):417–9.

850 62. Love MI, Huber W, Anders S. Moderated estimation of fold change and dispersion for RNA-seq
851 data with DESeq2. Genome Biol. 2014 Dec;15(12):550.

852 63. Mölder F, Jablonski KP, Letcher B, Hall MB, Tomkins-Tinch CH, Sochat V, et al. Sustainable data
853 analysis with Snakemake. F1000Research. 2021 Apr 19;10:33.

854 64. Perez-Riverol Y, Bai J, Bandla C, García-Seisdedos D, Hewapathirana S, Kamatchinathan S, et al.
855 The PRIDE database resources in 2022: a hub for mass spectrometry-based proteomics
856 evidences. Nucleic Acids Res. 2022 Jan 7;50(D1):D543–52.

857 65. Wolski WE, Nanni P, Grossmann J, d'Errico M, Schlapbach R, Panse C. prolfqua: A
858 Comprehensive R-Package for Proteomics Differential Expression Analysis. J Proteome Res. 2023
859 Apr 7;22(4):1092–104.

860 66. Barrett T, Wilhite SE, Ledoux P, Evangelista C, Kim IF, Tomashevsky M, et al. NCBI GEO: archive
861 for functional genomics data sets--update. Nucleic Acids Res. 2013 Jan;41(Database issue):D991-
862 995.

863

Figure 1

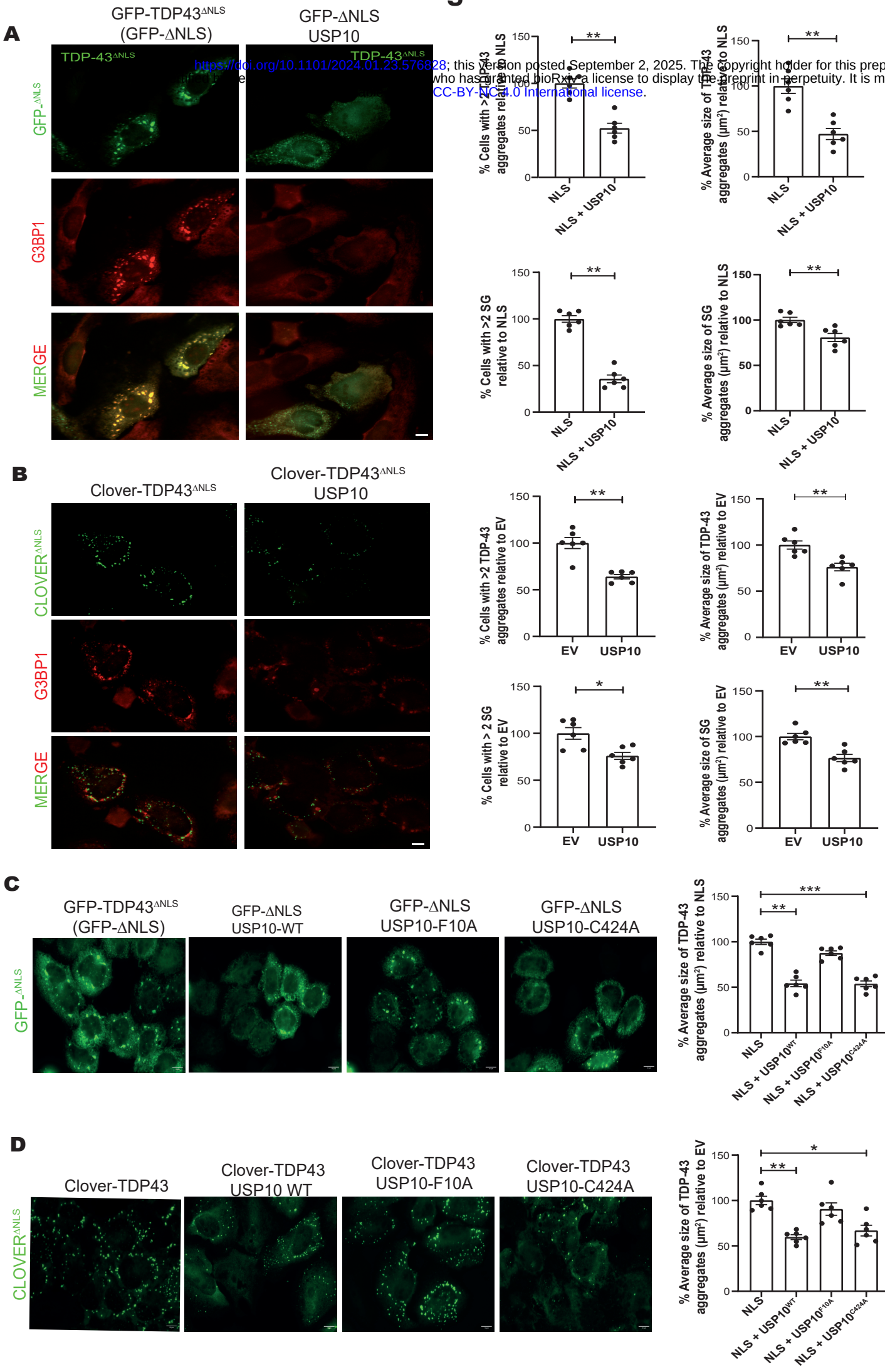

Figure 2

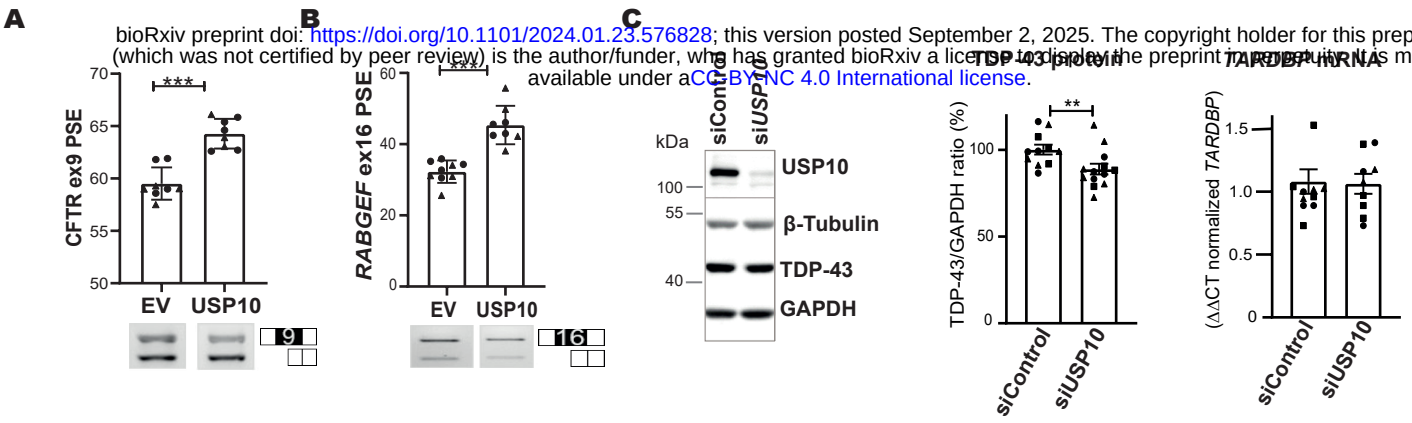

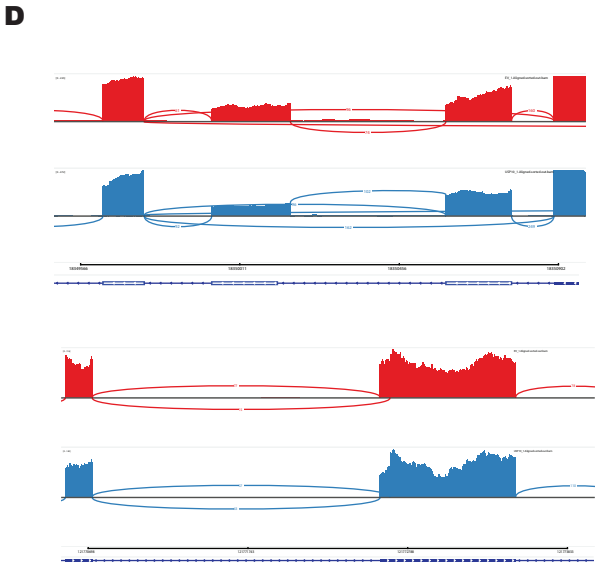

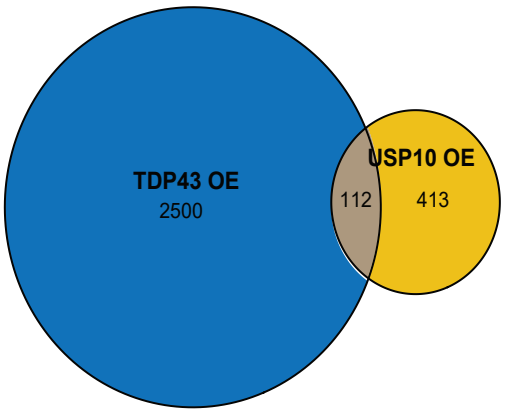

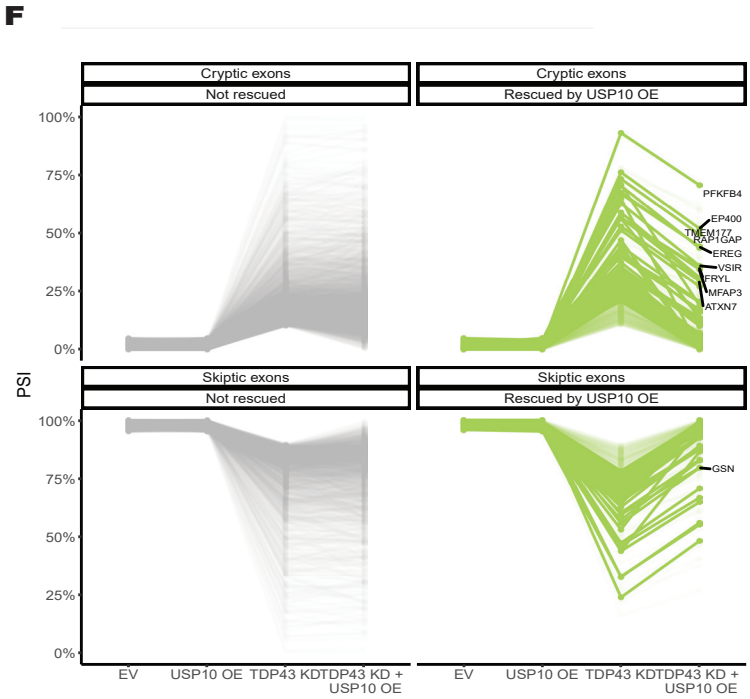

Figure 3